Fermi National Accelerator Laboratory

FERMILAB-Conf-91/137-E

QCD Tests at CDF*

The CDF Collaboration
Fermi National Accelerator Laboratory
P.O. Box 500
Batavia, Illinois 60510

Presented by
Paola Giannetti
Istituto Nazionale de Fisica Nucleare,
Pisa, Italy

May 1991

* Published Proceedings *Les Rencontres de la Vallee d'Aoste*, La Thuile, Italy, March 4-9, 1991.

Fermilab-CONF-91/137-E

QCD TESTS AT CDF

The CDF Collaboration*

Presented by Paola Giannetti
Istituto Nazionale di Fisica Nucleare,
Pisa, Italy

ABSTRACT

Recent analysis of jet data taken at the Fermilab Tevatron Collider at $\sqrt{S}$=1.8 Tev are presented. Inclusive jet, dijet, trijet and direct photon measurements are compared to QCD parton level calculations, at orders α_s^3 or α_s^2.The large total transverse energy events are well described by the Herwig shower Montecarlo.

* The CDF Collaboration

Argonne National Laboratory - Brandeis University -
University of Chicago - Fermi National Accelerator Laboratory -
Istituto Nazionale di Fisica Nucleare, Laboratori Nazionali of Frascati -
Harvard University - University of Illinois - The Johns Hopkins University -
National Laboratory for High Energy Physics (KEK) -
Lawrence Berkeley Laboratory - University of Pennsylvania -
Istituto Nazionale di Fisica Nucleare, University and Scuola Normale Superiore of Pisa -
Purdue University - University of Rochester - Rockefeller University - Rutgers University
Texas A&M University - University of Tsukuba - Tufts University -
University of Wisconsin

Published Proceedings Les Rencontres de la Vallee d'Aoste, La Thuile, Italy, March 4-9, 1991

Introduction

Data taken in 1988 and 1989 at the Fermilab collider resulted in significant advances in the study of high energy proton-antiproton collisions. The current CDF data sample, collected at $\sqrt{s}$ = 1800 GeV, corresponds to approximately 4.5 pb^{-1} of integrated luminosity. The high statistics available in CDF allows for more precise QCD tests than in the past. Two different approaches, almost complementary[1], are available to formulate theoretical predictions: the parton level calculation and the shower Montecarlo.

The parton level calculation evaluates in perturbation theory the matrix elements assuming that infrared physics will not affect the distributions. In section 2 of this paper different CDF measurements are compared to the relative parton level predictions:

a) The inclusive jet study will show the importance of a Next-to-Leading Order prediction[2] (NLO) compared to a simple Born level calculation.
b) Also the less inclusive two jet study will show the limitation of the Leading-Order (LO) calculation in describing the data behaviour.
c) Three jet events are compared to $O(\alpha_s^3)$ predictions based on tree level calculations of matrix elements that are sensitive to quark and gluon content.
d) Finally the direct photon cross section, which is not affected by parton fragmentation and is particularly sensitive to low x gluon structure functions, is compared to the NLO calculation.

The shower Montecarlos give a complete description of the process in the Leading Logarithmic Approximation. All the dominant infrared and collinear logarithms are accounted for, at any order in perturbation theory, while a correct treatment of the large-pt branchings is missing. Looking in the new energy range available to CDF, section 3 compares the largest E_t events to the Herwig shower Montecarlo[3].

1.1 Data Selection

The CDF detector has been described in detail elsewhere[4]. For these measurements, both jets in the central scintillator calorimeter and in the endplug gas calorimeter were used (fig.1).

For the inclusive jet and for the dijet analysis, the data were collected using single jet online triggers. These triggers basically required the presence of at least one energy cluster in the calorimeter with a transverse energy greater than, respectively, 20, 40, and 60 GeV. The 20 and 40 GeV jet triggers were pre-scaled.

The data for the three-jet analysis were collected requiring a total transverse energy in the calorimeter greater than 120 GeV. The same kind of trigger, but with two thresholds, was used for the study of high transverse energy events: total transverse energy greater than 120 or 150 GeV.

A prescaled low Pt trigger (Pt > 10 GeV) and a high Pt trigger (Pt > 23 GeV) were used to

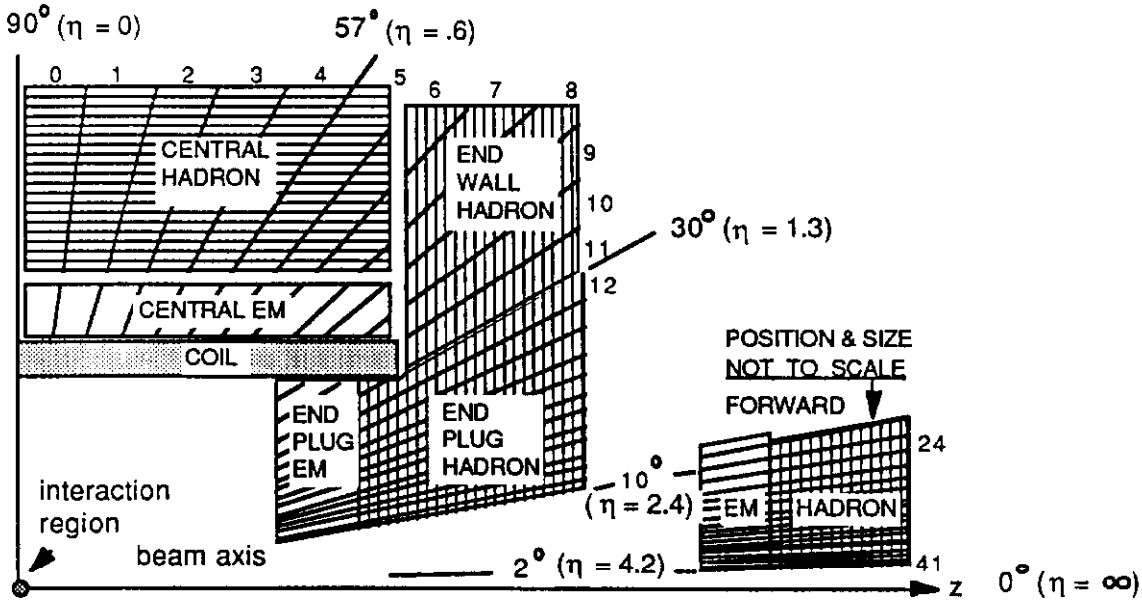

Fig. 1: The CDF calorimeter

select the direct photon sample. The photon cluster was also required to have a low hadronic energy fraction ($E_t^{had}/E_t^{em} < .125$) and to be isolated; the extra energy inside a cone of radius $R=(\Delta\eta^2 + \Delta\phi^2)^{1/2} = 0.7$ (where η and ϕ represent pseudorapidity and azimuthal angle) centered on the photon was required to be less than 15% of the neutral cluster energy.

1.2 Jet Definition

In the past the experimental jet definition was oriented to reproduce as much as possible the Born Level approximation of the hard process. At the leading order the final state is

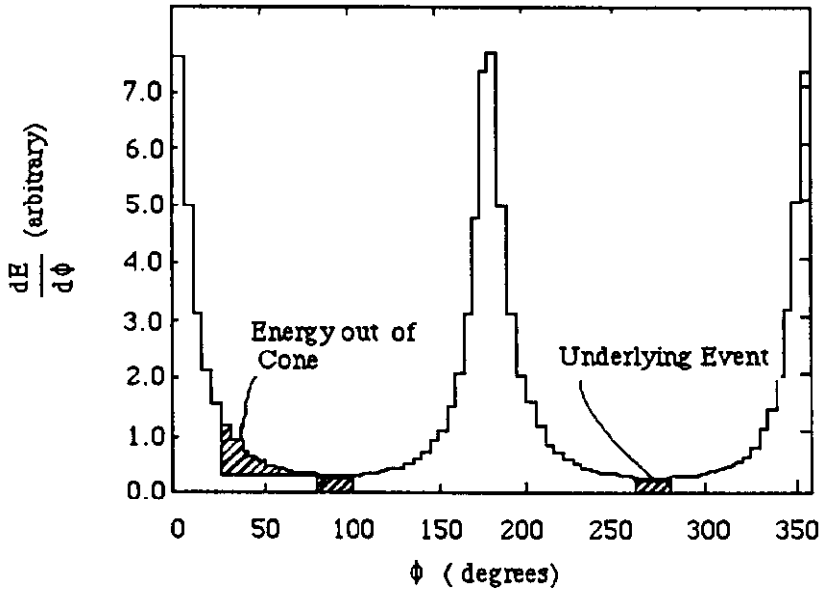

Fig. 2: Energy flux around the jet axis

caracterized by 2 partons of zero size in the $\eta - \phi$ space and opposite in the transverse plane.

The jet energy measurement (affected by gluon radiation, fragmentation and underlying event) was corrected to try to reproduce the simple theoretical LO approximation.

Fig 2 shows the average energy flow around the jet axis as a function of the distance ϕ from the jet axis. The plot is obtained using clean 2 jet events, that is excluding events where radiation produced a third jet. The density of energy at 90° from the jet axis was taken as a measure of the average energy density of the underlying event and subtracted from the jet energy ('underlying event correction'), while the amount of energy out of the clustering cone and above what expected from the underlying event was considered as belonging to the original parton and added to the jet energy ('out of cone correction').

This procedure fits the data analysis to the specific order the theory is calculated to. The improvement of theoretical calculations, which makes available higher order predictions, suggests the use of a more general procedure, independent of the present level of the theoretical technique. The NLO calculation allows for cases when a third parton is present in the final state.

Fig. 3 shows that indeed measurement and theory have stronger similarities in the NLO approximation. In the experiment we see energy clusters well separated but near in the η–ϕ space; also the theory provides partons that can be near in the η–ϕ space. Depending on the choice of the cone size, clusters and partons can be merged together and the cross section would change accordingly. The theoretical calculation should reproduce the cross section cone size dependence observed in the measurement.

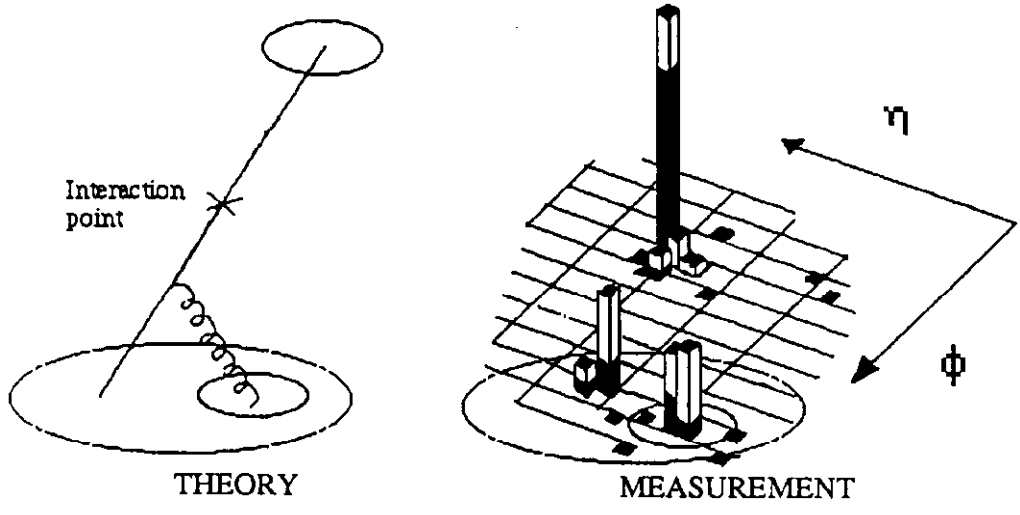

Fig. 3: Jets as seen by NLO theory and by experiment

The Snowmass accord[5] is an attempt to fix a standard jet definition not only unifying the different experimental approaches (UA1, UA2, CDF) but also providing an empirical definition of jet that is easily reproduced by the theoretical calculation. Jets are clustered with a

fixed size cone algorithm[6]. The algorithm also gives the momentum of each jet, assuming a massless particle for each calorimeter tower belonging to the cluster. The jet transverse energy and centroid are defined as:

$$E_t = \sum_{R_i \le R_0} E_{ti}$$

$$\eta = \frac{1}{E_t} \sum_{R_i \le R_0} E_{ti}\eta_i \qquad \phi = \frac{1}{E_t} \sum_{R_i \le R_0} E_{ti}\phi_i$$

where i indicates the i^{th} calorimeter cell in the case of the experiment and the i^{th} parton in the case of the theory.

The 'out of cone corrections', applied in the past become now incompatible with the NLO calculation and have been applied any more. For convinience we dropped the 'out of cone corrections' also in those cases, as the two-jet cross section, for which NLO calculations are not yet available. This choice provides a simple standard for all jet measurements and will allow in the future to compare our results to NLO calculations as soon as they are available. For the time being, when comparing the data to the LO theory, losses out of the cone are accounted for a contribution to the theoretical systematic error.

Also the underlying event correction is affected by an uncertainty. It is uncorrect to assign all the energy density seen at 90° from the 2 leading jets to the underlying event[7]. This energy density is actually larger than the one observed in minimum bias events, a clear indication that there is a contribution from the hard scattering. In the following we apply the underlying event correction only for some measurements, but we always take into account the appropriate systematic uncertainty.

1.3 Detector Response

The effects of smearing due to finite energy resolution and of energy degradation due to calorimeter response non-linearities, uninstrumented regions of detector, etc., distort the measured spectra. In order to take into account these effects, a Montecarlo was used[8]. It was tuned to reproduce the experimental jet fragmentation and the calorimeter response to single pions, as measured in the test beam and using isolated momentum analyzed hadrons in the actual data. The detector effects were taken into account when comparing data to theoretical predictions, either unfolding the data or folding the theory with the detector response[10] to jets. The major sources of systematic error on the jet energy scale result from uncertainties in calorimeter response and fragmentation tuning in the Montecarlo. The systematic uncertainties on the jet cross section are tipically 22% and independent of E_t for values of E_t above 80 GeV. Below 80 GeV, they rise as high as 60% at 25 GeV.

2.1 Inclusive Jet Production

The first important feature of the NLO calculation is the reduced dependence of the cross sections on the choice of the renormalization scale. The dominant theoretical uncertainty is due to differences in the structure functions, while when using the Born Level cross section, the choice of the renormalization scale gives a not negligible contribution. For our inclusive cross section measurement, jets in the central pseudorapidity region ($0.1 < |\eta| < 0.7$) were selected. Cosmic ray background was removed rejecting jets caracterized by showers out of time with the beam crossing or by unrealistic energy deposition, and rejecting events with large missing E_T.

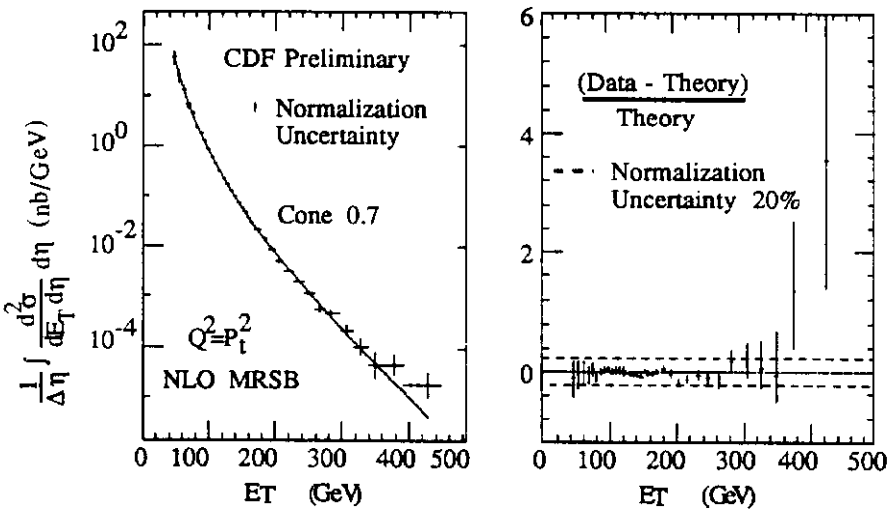

Fig. 4: Inclusive jet cross section compared to next-to-leading order QCD. The plot on the right shows the residuals on linear scale

Fig. 4 shows the differential cross section as a function of E_t for a cone size of 0.7 compared to a NLO QCD calculation (solid line). The data were corrected for the detector response, the underlying event energy was subtracted, and no out-of-cone correction was applied. The error bars on the data points represent the statistical and the E_t dependent systematic errors added in quadrature. The QCD prediction shown in fig. 4 uses the structure function MRSB[9] and $Q^2=P_t^2/4$. This prediction was normalized to the data by fitting a global normalization factor. The normalization factor is a small positive correction of 6% to the theory. The agreement is good over 7 orders of magnitude in cross section.

The plot in fig. 5 shows the cross section dependence on cone radius. The cross section has been measured as a function of R for 100 GeV E_t jets. The error bars on the data points represent the statistical errors.

The data have a behaviour similar to QCD, with a steeper dependence on the cone size than what α_s^3 calculations would predict. This may suggest the importance of still higher orders. However the α_s^3 calculation appears to be able to qualitatively reproduce the effect.

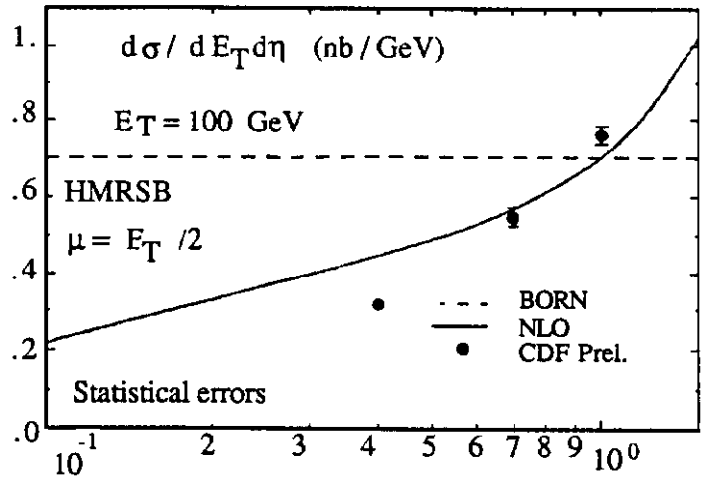

Fig. 5: Cross section at E_t=100 GeV as function of the clustering cone size

At the Born level, jets correspond to single partons that have zero widths in the η–ϕ space. The QCD α_s^3 calculation provides 2 partons near in the $\eta - \phi$ space. This can be considered as a first step in the description of the jet shape. At sufficient high energies the fragmentation effects may become negligible and the jet shape should be reproducible by perturbative QCD alone. Indeed QCD fragmentation models based on parton showers were shown to be succesfull in describing jet features. The comparison of the jet shape with the prediction of the α_s^3 calculation shows how well a single extra parton in the final state can explain the jet dimension. We have measured the P_t flow around the jet axis for jets of transverse energy 100 GeV. We define a *shape (r)* function (fig. 6) by measuring the P_t fraction inside a cone of radius r, smaller then the jet cone size R_0. This function is normalized to be equal to 1 for $r=R_0$ and, of course, goes to zero for $r\to 0$. The jet axis is defined by the calorimeter with a clustering cone radius R_0=1.

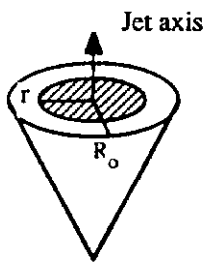

$$\text{shape}(r) = \frac{\int_0^r \rho(r')\,dr'}{\int_0^{R_0} \rho(r')\,dr'}.$$

Fig. 6: Definition of the shape (r) function

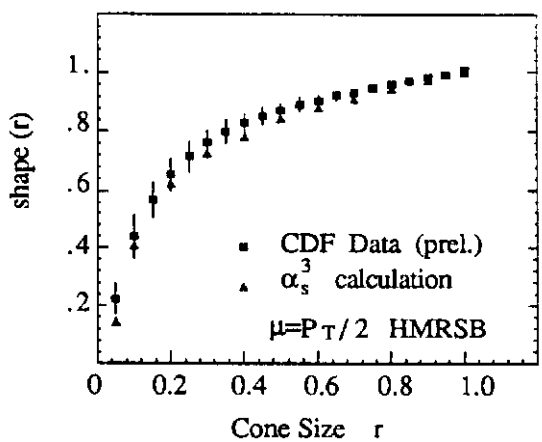

Fig. 7: Jet shape - Data versus NLO

Tracks found in the central tracking chamber (CTC)[4] were used to calculate the P_t flow. We thus assume that the neutral particle P_t flow is the same as for charged particles. The use of CTC tracks improves the spatial resolution and simplifies the problems caused by the non-

linearity of the calorimeter.

If ρ_t (r') = (1/N) Σ dP_t/dr' (where dP_t is the scalar sum of the p_t's of the tracks pointing to the anular region between r' and r'+dr', the sum runs over all jets and N is the number of jets) is the average P_t density, the shape function is defined as

$$\text{shape (r)} = \frac{\int_0^r \rho\,(r')\,dr'}{\int_0^{R_0} \rho\,(r')\,dr'} .$$

Jets were selected in the central rapidity region $0.1 < |\eta| < .7$, and with transverse energy in the range $95 < E_t < 120$ GeV. Very unbalanced events are rejected to avoid badly measured jets and cosmic rays. Finally, quality cuts are applied to select good 3-dimensional tracks.

Fig. 7 shows both the theory and the data corrected (7% in the jet core) for track efficiency. The systematic error, mainly due to jet axis determination, is shown on the data points. The theoretical uncertainty, mainly due to the renormalization scale choice, is not shown, but it is of the same order as the uncertainty on the data. The agreement is surprisingly good. It seems that a third parton in the final state can give a good description of the jet shape.

2.2 Dijet Production

Additional tests of QCD involve the study of dijet events. We measured the dijet invariant mass spectrum. The two leading jets in an event are used to define the dijet system. In their center of mass frame, the two jets are back to back and they are described by the dijet invariant mass M_{jj} and by the scattering angle θ (the angle between the jets and the incoming partons).

The dijet invariant mass was calculated as $M_{jj} = [(E_1+E_2)^2-(\mathbf{P}_1+\mathbf{P}_2)^2]^{1/2}$, where E_i and $\mathbf{P}_i$ are the measured energies and momenta of the two leading jets. Since the next-to-leading order QCD predictions are available only for the inclusive jet production, the comparison is done with a leading order prediction. Still no out of cone or underlying event corrections have been applied to the jet energies, but the related theoretical uncertainties on the predicted cross section are used when comparing data to theory. Moreover, instead of correcting the data for the finite detector resolution, in this case the theoretical predictions were smeared using the detector response as a function of M_{jj} as derived in the Montecarlo[10].

Fig. 8 shows $d\sigma/dM_{jj}$, integrated over the pseudorapidity range $|\eta| < 0.7$, for two chices (R=1 and R=0.7) of jet cone size. The crosses represent the experimental points with their bin widths and statistical errors. The two solid lines on each plot define a band of uncertainty in the theory. This was obtained as the envelope of different predictions using different parametrizations for the structure functions, namely EHLQ, DO, DFLM, HMRS, MT [11,15] and varying the Q^2 in the range $0.5P_t^2 < Q^2 < 2P_t^2$. The comparisons are on absolute scale and the theoretical predictions are not normalized to the data.

To perform a shape test, we also normalized the theoretical predictions to the data by fitting a global normalization factor, taking into account the systematic uncertainties. Table 1 shows

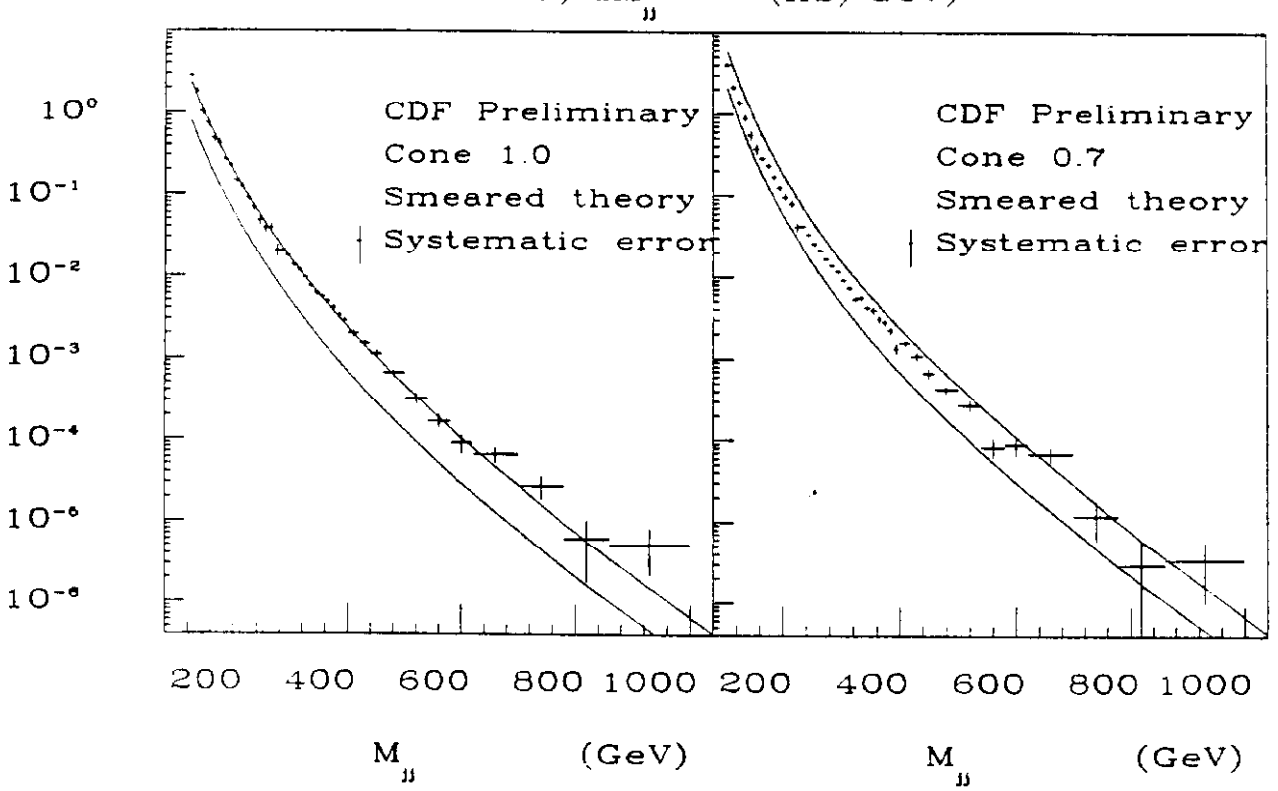

Fig. 8: Comparison on Absolute Scale

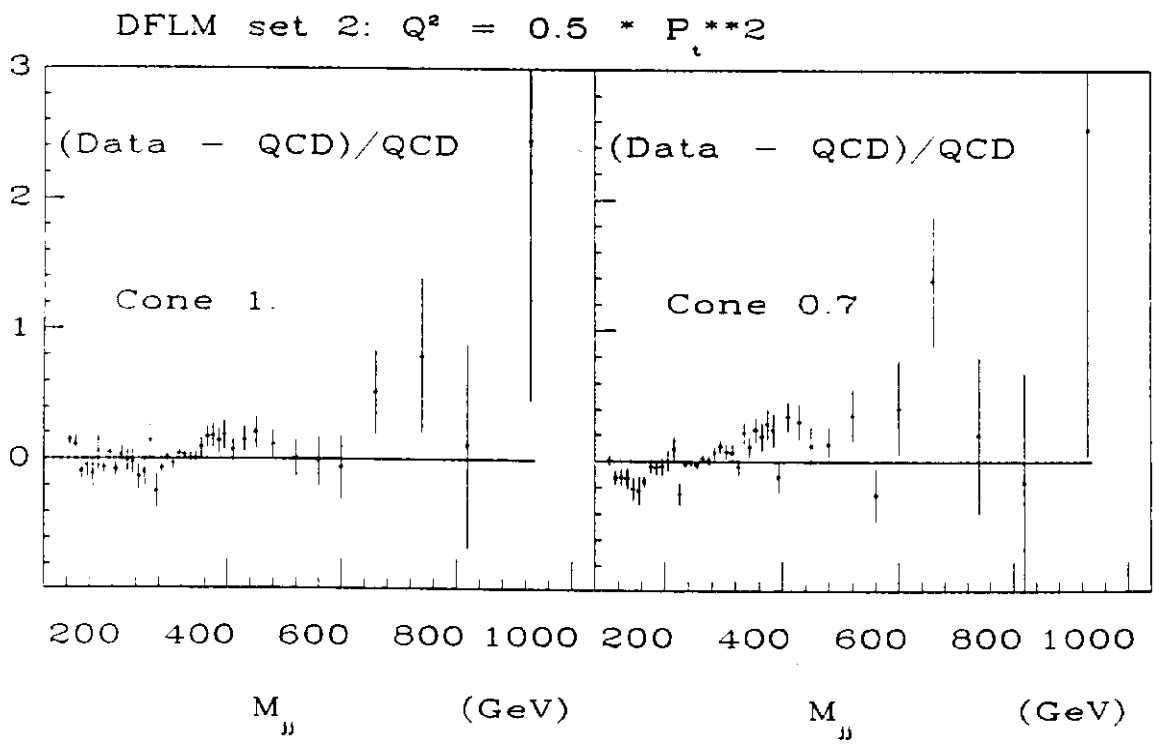

Fig.9: Shape Test − Same theory fit on both mass spectra

the corresponding confidence levels. Basically all structure functions and Q^2 scales are in agreement with the measurement obtained with the cone size R=1, while all of them give a poor fit to the measurement obtained with the smaller cone. This effect could come from higher order diagrams that can cause bremsstrahlung out of the smaller cone. These losses could affect not only the absolute normalization of the measurement (as it can be seen in fig. 8), but also the shape of the distribution. It will be interesting to see if the NLO predictions will explain this effect. As an example fig. 9 shows, on linear scales, the quantities (Data-Theory)/Theory for DFLM set 2 with Q^2=.5 P_t^2, fitted on the two measurements. The solid horizontal line represents the theory and the points, with statistical errors only, show the deviations of the data. The cone 1 measurement shows a steeper dependence on M_{jj} than the cone 0.7, the latter having a slope inconsistent with the theory.

Table 1: L.O. QCD vs. CDF Mjj Spectrum Confidence Levels (%)
CDF Preliminary - Systematic uncertainties included

Q^2 / P_t^2 =	1	2	0.5	1	2	0.5
Structure Functions	CONE		1.0	CONE		0.7
DFLM Λ_{QCD}=101	48	46	47	1	1	<1
DFLM Λ_{QCD}=173	54	52	54	1	1	2
DFLM Λ_{QCD}=250	50	52	53	2	2	2
DO1	51	51	47	2	1	<1
DO2	49	48	48	2	2	2
EHLQ1	40	38	40	<1	<1	<1
EHLQ2	24	21	25	<1	<1	<1
HMRSB	46	48	47	2	1	1
HMRSE	46	46	39	3	4	4
MT Λ_{QCD}=155	57	58	54	3	3	2
MT Λ_{QCD}=187	56	56	56	2	2	1
MT Λ_{QCD}=191	66	65	64	5	6	6
MT Λ_{QCD}=212	62	61	59	3	4	3

2.3 Three Jet Events

The large available statistics allows a detailed comparison between the α_s^3 tree level predictions and three jet events. At tree level the matrix elements[16] are sensitive to the relative quark/gluon content in the beams. Two relevant subprocesses examined here involve all gluons or two quarks and three gluons. The differences in these subprocesses reflect the different dynamics respectively associated with the three gluon vertex and the quark-gluon vertex (differences in the spins and couplings). An example of gluon-quark differences is that the process gg→ggg has a steeper cross section in the collinear limit than the process qqbar→ggg .

We adopt the same conventions used by UA1 [17] to describe three jet events in their center of mass frame. As shown in fig. 10 we label the three jets with numbers 3 to 5 according to decreasing energy, and use the numbers 1 and 2 for the initial state partons. We define three angles: θ as the angle between jet 3 and parton 1, ψ as the angle between the event plane and the plane defined by jet 3 and parton 1, and φ as the azimuth of jet 3. Then we define the energy fractions of the three jets $x_i = 2E_i/M_{3j}$ (where M_{3j} is the three jet invariant mass). The degree of freedom φ is of no dynamical interest because of the simmetry around the beam axis. For a pure phase space decay, i.e. constant matrix element, the differential cross section $d^4\sigma/dx_3dx_4d(\cos\theta)d\psi$ is constant at fixed M_{3j}.

Three jet events are selected by requiring at least three calorimetric clusters with $E_t > 15$ GeV, well separated from each other ($\Delta R \geq 0.85$ in η–ϕ space) and with pseudorapidity $|\eta|<3.5$. In addition, M_{3j} is required to be greater than 250 GeV. Additional cuts are imposed to avoid problems both in theoretical calculations (infrared divergencies) and in measurement (inefficiency, confusion with beam jets): $x_3 < 0.9$, $|\cos\theta| < 0.6$, $30°<|\psi|<150°$.

The theoretical distributions have been obtained generating 3 partons in the final state according to the tree level matrix elements, fragmenting them into jets and simulating the detector response. The same analysis applied to the data is repeated on simulated events.

The measured cross section within the above defined acceptance cuts is 1.2 ± 0.4 nb (the main error is systematic and is due to the energy scale uncertainty). The QCD predicted cross section is 1.0 nb with an uncertainty of 50% due to structure function and renormalization scale uncertainties.

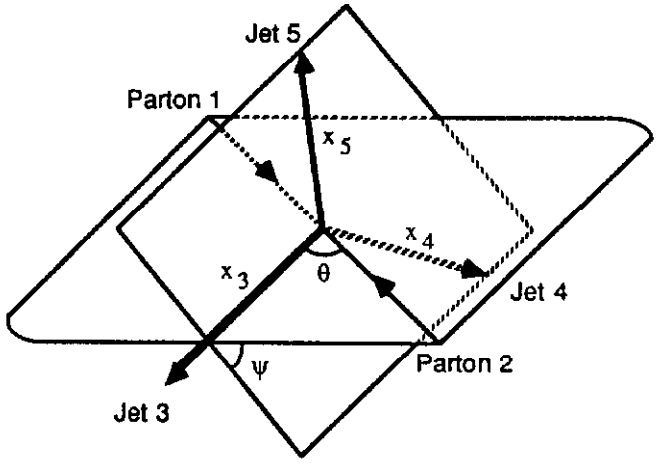

Fig. 10: Kinematics and labelling of three-jet events.

To understand the contribution of gluons in the initial state, we compare the data to α_s^3 tree level predictions (*full QCD* for brevity) as well as to the partial contributions from processes initiated by qqbar only (*qqbar QCD*).

The measured distributions in x3 and x4, with their statistical errors, are compared in fig.11 to phase space, to full QCD and to qqbar QCD. Data clearly prefer the full QCD prediction over processes involving only qqbar in the initial state and are inconsistent with pure phase

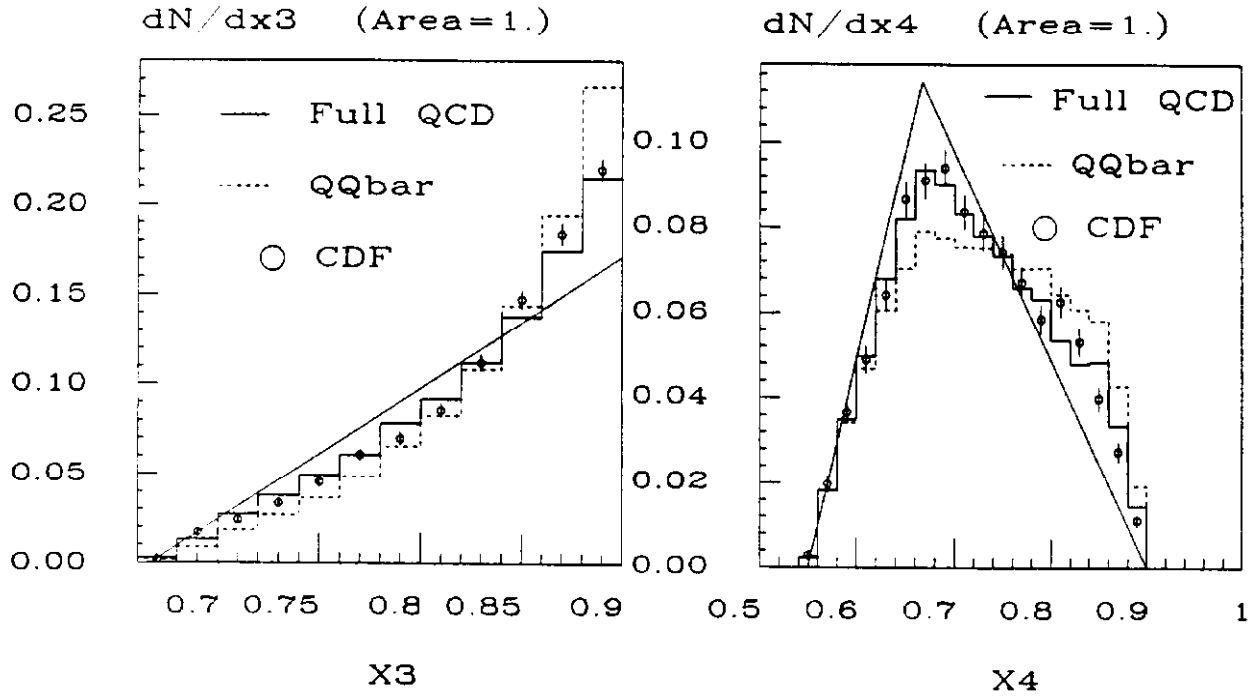

Fig.11: Jet Energy Fractions x3 and x4 (CDF Prel.)

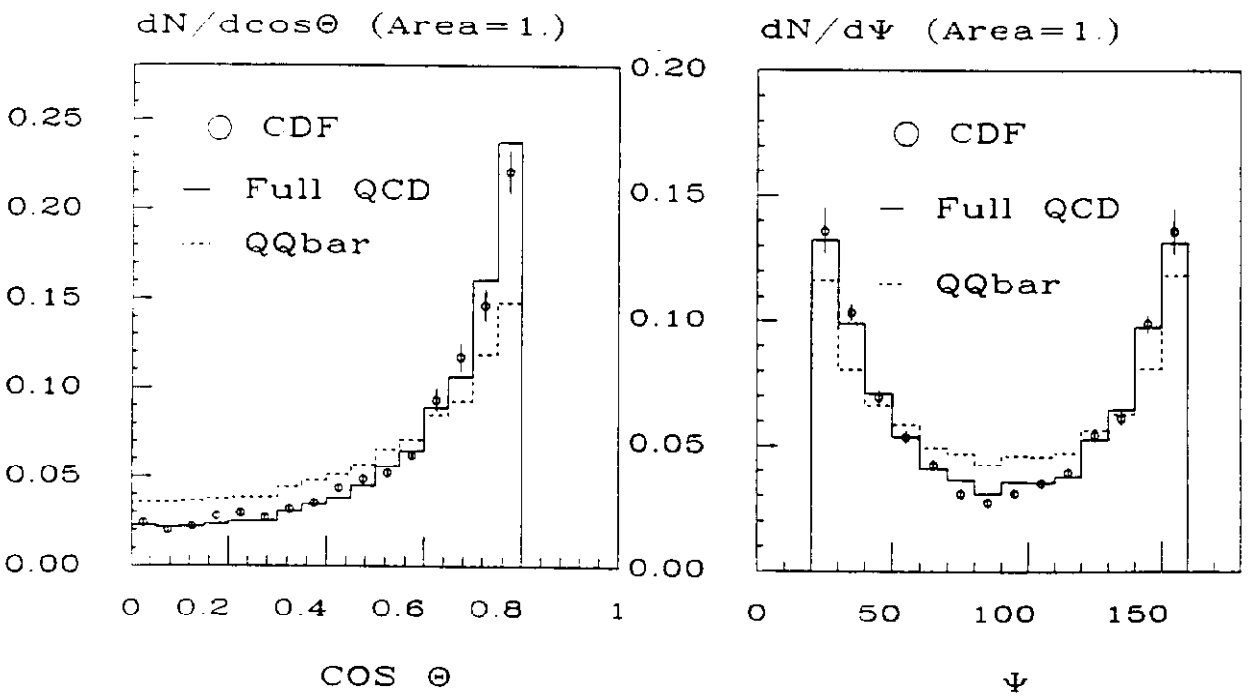

Fig.12: Angular distributions for 3-jet events
(CDF Preliminary)

space.

Fig. 12 shows the angular distributions.

The cosθ distribution shows the forward peaking expected for processes dominated by the t channel exchange of vector particles. There is an obsarvable difference between the full QCD and the qqbar initiated process. Data again clearly indicate that processes with gluons in the initial state should be included.

An angle ψ almost equal to 0 or π corresponds to the condition of parallel planes where the radiated final state jet, maintaining costant all the other parameters, has the minimun angular distance from the incoming partons. The two corresponding peaks in the plot are the effect of singularities associated with the emission of radiation from the incoming partons. As expected from the gluon and quark splitting functions, the radiation at small angles has a larger contribution from gluons than from quarks in the initial state. Again data prefer the full QCD prediction.

The 4 distributions of figg. 11, 12 are used in a combined fit where the fraction of events generated by the qqbar initial state is the free parameter. The best value for the qqbar fraction is a small number $3\%^{+12\%}_{-3\%}$ compatible with the theoretical prediction $11\% \pm 4\%$.

2.4 Direct Photons

In CDF we have two methods to separate direct photons from π^0 and η decays [18].

The first uses a shower profile measurement with a wire chamber at 5 radiation lengths in the electromagnetic calorimeter. A single γ showering in the EM calorimeter is characterized by a narrow cluster whose profile is measured with electrons at the test beam. Two nearby photons from a π^0 or η decay have a wider profile and produce a statistically larger χ^2 when fit to an electron shower profile. We select a γ enriched sample by imposing the cut $\chi^2<4$. Knowing the χ^2 distributions for signal and background from the Montecarlo, we can estimate their relative efficiencies. In a recent work we have gained new confidence on the efficiencies calculated from Montecarlo. We selected η's decaying into two well separated γ's to measure the χ^2 distribution of single photons and we select $\rho^{\pm}$ decaying into $\pi^{\pm}$, π^0 to measure the χ^2 distribution for a π^0 enriched sample. Fig. 13 shows the η and ρ mass peaks and the χ^2 distributions. The simulation (dashed lines) shows a good agreement with the data.

The second method measures the direct γ flux by counting the number of conversions produced just outside the tracking chambers and detected by the central drift tubes in front of the coil[18]. The amount of conversion material is about 18% radiation length overall. For a single γ the conversion probability is $10 \pm 2\%$ and roughly twice for π^0 which decays to two γ's.

A partial data sample was analysed (45. nb^{-1} for E_t threshold of 10 GeV and 1.6 pb^{-1} for E_t threshold of 23 GeV). The direct γ cross section is shown in fig. 14. The measurement from

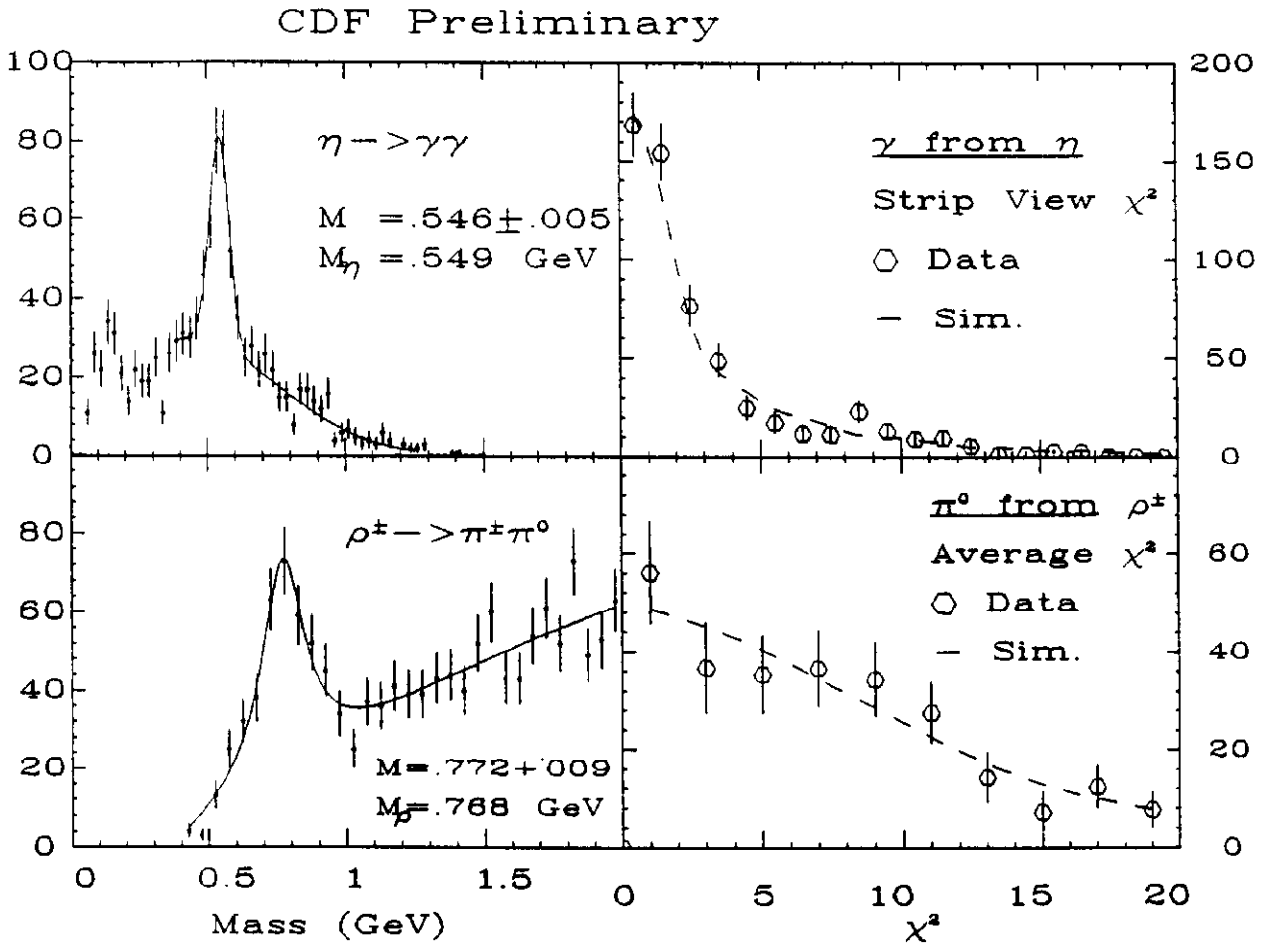

Fig. 13: Measuring χ^2 of γ and π^0 from data

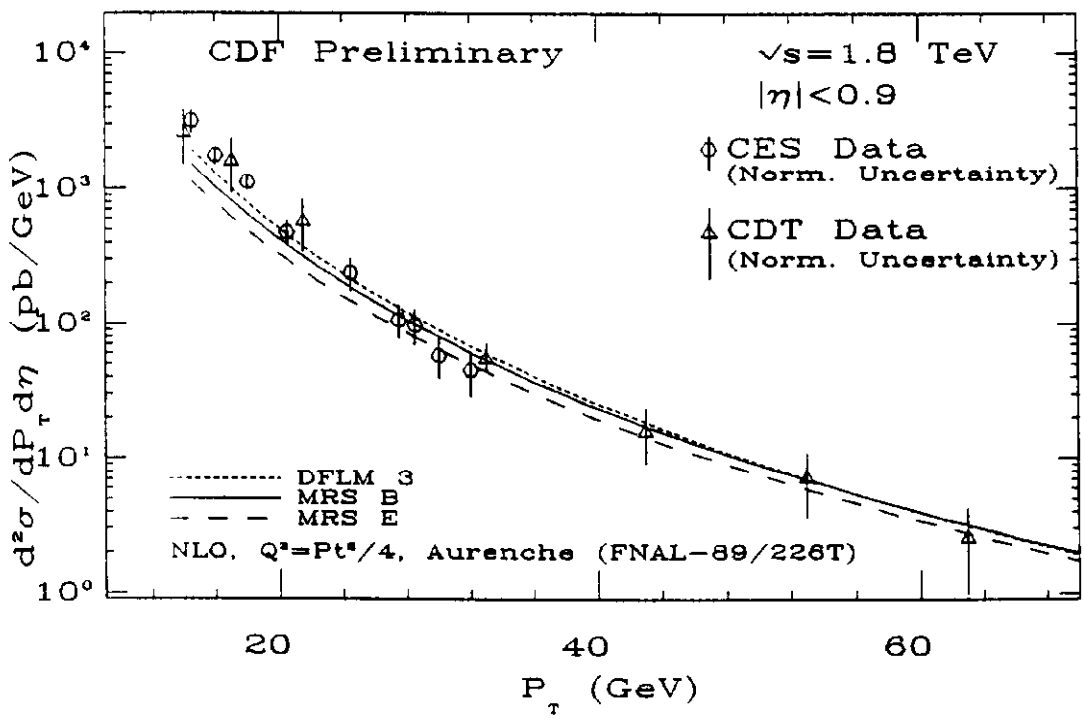

Fig. 14: Direct Photon Cross Section

the shower profile method is more precise, but cannot be extended over Et≈35 GeV, because an energetic π^0 looks like a single γ in the chambers. One sees in fig. 14 that the two methods agree in the overlap region. These results are compared to NLO calculation[19]: the data exhibit a somewhat steeper dependence on P_t than the theory. It is still unclear whether the theoretical uncertainties can accomodate for this deviation (bremsstrahlung diagrams are calculated only at order $\alpha\alpha_s$ rather than $\alpha\alpha^2_s$ and their contribution is significant at low P_t), or a softer than expected gluon distribution is being observed.

3.1 Very Large Total Transverse Energy Events

To understand if the new energy region available to CDF is consistent with QCD expectations, we compare the events with very large total transverse energy (ΣE_t) observed by CDF to the Herwig (version 4.3, DO1 structure function with Λ_{QCD}=200 MeV) shower Montecarlo. This comparison is also a test of the leading-log-approximation implemented in shower Montecarlos.

The high ΣE_t events (4.0±0.3 pb^{-1}) were selected requiring ΣE_t>400 GeV (uncorrected energy), where the sum runs over all calorimeter towers with E_t>500 MeV.

Cosmic rays and beam halo events were rejected requiring the out-of-time energy deposition in the central hadronic calorimeter to be small, or requiring a small missing transverse energy ($\not\!\!E_t/\sqrt{\Sigma E_t}\geq 6$). Finally, using the VTPC, events with multiple vertices were identified and rejected: of 306 events 27 events had at least 2 vertices. The systematic uncertainties are presently under study.

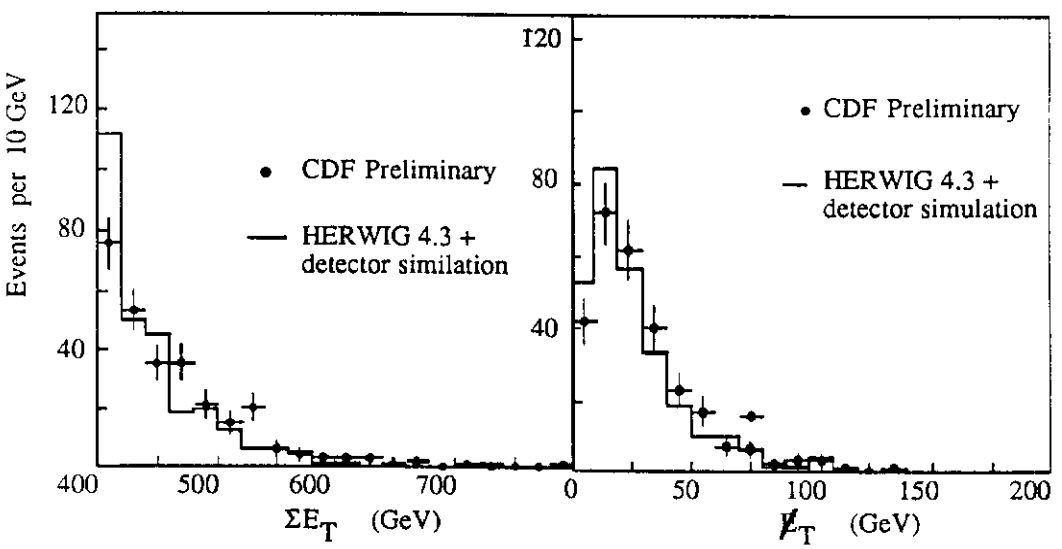

Fig. 15: Total Transverse Energy

Fig. 16: Missing Transverse Energy

All the 279 events of the final sample show jet activity. In figg. 15, 16 the observed ΣE_t distribution and the missing-E_t distribution are compared with QCD expectations. QCD seems able to account for the tail of the two spectra.

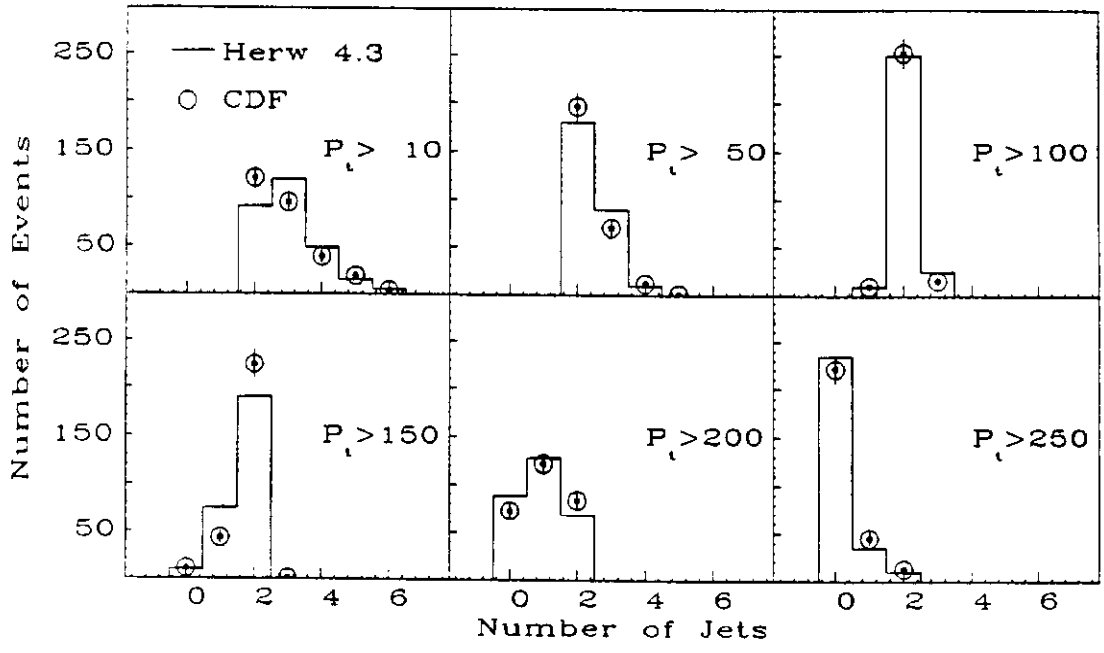

Fig. 17: Jet Multiplicity (CDF Preliminary)

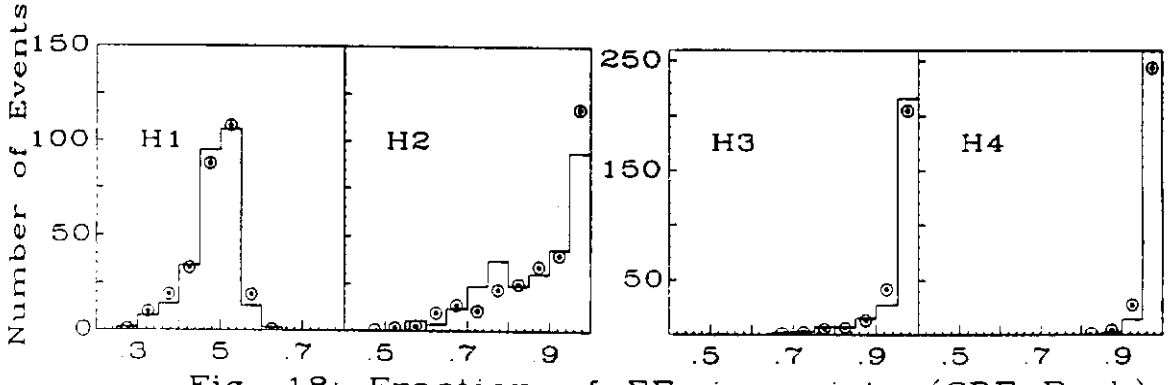

Fig. 18: Fraction of ΣE_t in n jets (CDF Prel.)

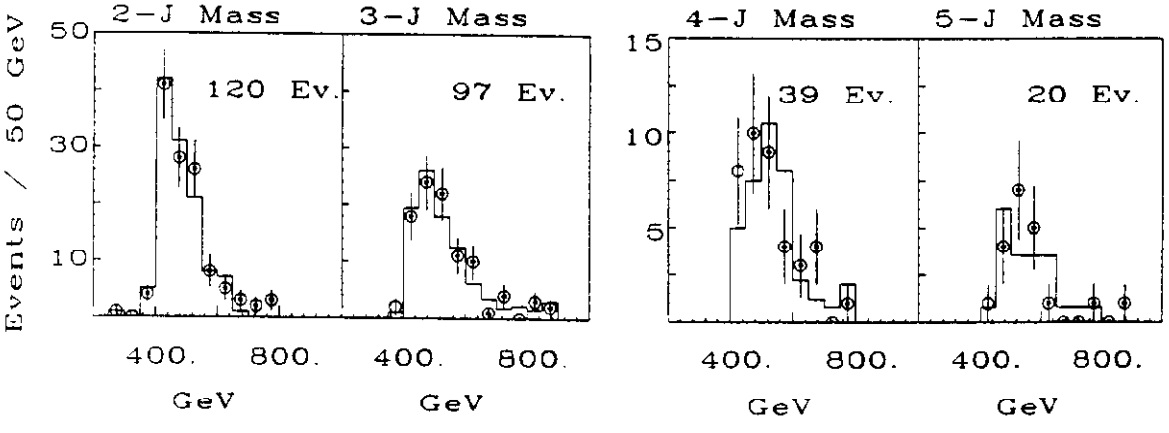

Fig. 19: Multi-Jet Mass Spectra (CDF Preliminary)

Fig.17 shows the distribution of the number of jets observed in the event above a certain threshold of P_t, for different thresholds. For low thresholds the jet multiplicity is high, while for a 100 GeV P_t threshold most of the events look like two-jet-events. Jets are reconstructed using a cone size 0.7 and selected requiring $|\eta|<2$ and $p_t>10$ GeV. The leading-log-approximation implemented in Herwig appears to give an adequate description of the rate of additional jets arising from higher-order processes.

Fig. 18 confirms the idea that most of the hard scattering energy is collected by the two leading jets, even if the jet multiplicity can be high. In this figure we plot the relative fraction of total ΣE_t carried by the n leading jets:

$$H_n = \frac{\sum_{j=1}^{n} E_{Tj}}{\Sigma E_T}$$

where the scalar sum in the numerator is over the n leading (highest p_t) jets reconstructed in the event (no p_t and η cuts were applied to jets before computing H_n). H_1, the fraction of transverse energy belonging to the leading jet, clearly peaks to 50% while H_2 peaks to 100% confirming the two-jet dominance in high-ΣE_t events. The long H_2 tail almost disappears when including the 3^{th} and 4^{th} jets in the sum.

The two-jet, three-jet, four-jet, and five-jet mass distributions are shown in fig. 19 for those events containing two, three, four and five jets with $|\eta|<2$ and $p_t>10$ GeV. Clearly multi-jet properties find a good approximation in Herwig.

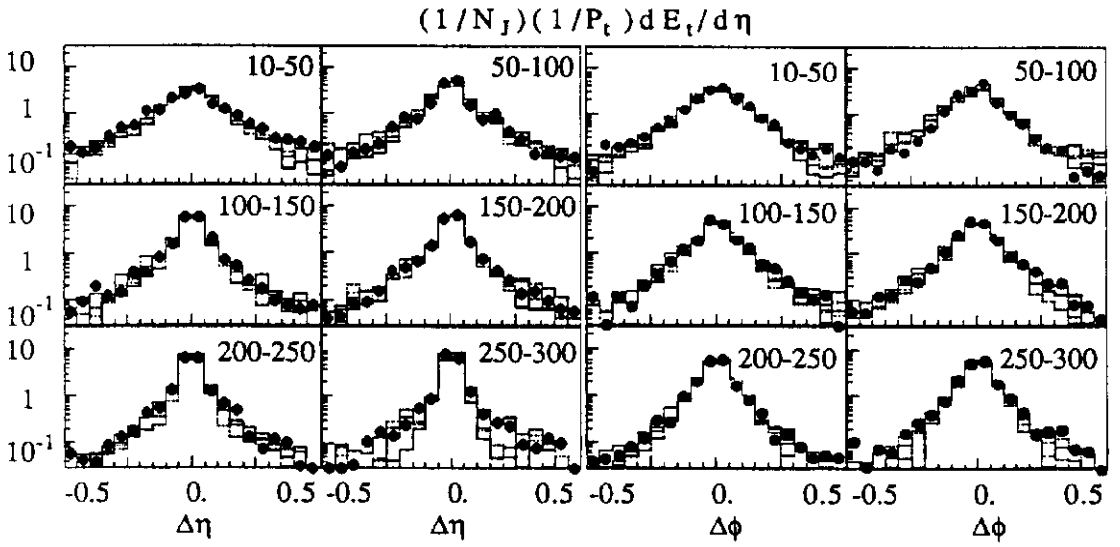

Fig. 20: E_t flow about the Jet Axis in the η-ϕ space for different P_t's

We have seen in the paragraph 2.1 that the α_s^3 calculation is able to explain the jet shape for jets with E_t=100 GeV. We now show in fig. 20 that the average jet profile, that is the E_t flow around the jet axis, is also well described by the leading-log-approximation.

Different plots correspond to different jet P_t's and show the trend of the profile to shrink as

the jet P_t increases.

4.1 Summary

a) The inclusive jet can now be compared to a NLO QCD prediction. We measured the inclusive jet cross section $d\sigma/dE_t$ at $\sqrt{s}$ = 1.8 TeV and in the E_t range from 30 to 400 GeV. We observe a good agreement with the NLO calculation over 7 order of magnitudes. We see some difference between theory and data on the cross section dependence by the cone size. The α_s^3 calculation seems to explain the jet transverse shape with just an extra parton in the final state.

b) The two-jet event data can only be compared to a LO calculation.We measured the dijet mass spectrum using two different cone sizes in the clustering algorithm: R=1 and R=0.7. The available LO theoretical predictions agree well with the cone 1 measurement, but gives a poor description of the cone 0.7 spectrum. It will be interesting to see if the NLO predictions, which are expected to be available soon, will explain this effect.

c) The three jet event topology has been studied. Data are in agreement with α_s^3 tree level predictions and show preference for gq and gg initiated processes. From these data, we have been able to estimate the fraction of events initiated by qqbar.

d) We showed an improved analysis of our photon measurement. The inclusive spectrum shows a steeper dependence on E_t than the NLO predictions. This may be attributed to an incorrect input gluon structure function. However no conclusion on gluon structure functions is possible until theoretical uncertainties affecting the low P_t region are understood.

e) CDF gives us the possibility to probe a new energy region. Comparing the high-ΣE_t events to Herwig we come to the conclusion that QCD effects dominate also this energy region. Indeed the leading-log-approximation is able to reproduce reasonably well all features of this high energy event sample.

References

[1] M. Mangano, Proceed. of the 8th Topical Workshop on P-Pbar Collider Physics (1989), Castiglione della Pescaia - Italy, 104

[2] S.D. Ellis et al., ETH-TH/90-3 (1990); F. Aversa et al., LNF-90/012 PT (1990).

[3] G. Marchesini and B. Webber, Nucl. Phys., **B310** (1988) 461

[4] CDF Collaboration, Nucl. Instr. and Meth. **A267** (1988) 249, 257, 272, 280, 301, 315, 330; **A268** (1988) 24, 33, 41, 46, 50, 75, 92.

[5] J. Huth et al., Fermilab-CONF-90/249-E and Proceed. of the Summer Study on High Energy Physics (1990), Snowmass - Colorado

[6] D. Brown et al., CDF Internal Note **605** (1988).

[7] G. Marchesini and B.R. Webber, NSF-ITP-88-67, (1988)

[8] D. Brown et al., CDF Internal Note **753** (1988); .. CDF Internal note **1066**; .. CDF Internal Note **1131**.

[9] A.D. Martin et al., Phys. Rev. **D37** (1988) 1161.

[10] M. Dell'Orso et al., CDF Internal note **1056** (1989).

[11] E. Eichten et al., Rev. Mod. Phys. **56** (1984) 579.

[12] D. Duke and J. Owens, Phys. Rev. **D30** (1984) 49.

[13] M. Diemoz et al., Z. Phys. C39 (1988) 21.

[14] P.N. Harriman et al., RAL preprint 90-007 (1990)

[15] W. Tung and J.G.Morfin, Fermilab-PUB-90/74, IIT-PUB-90/11

[16] Z. Kunszt , E. Pietarinen, Nucl. Phys. **B164** 45 (1980); T. Gottschalk, D.Sivers, Phys. Rev. **D21** 102 (1980); F. Berends et al., Phys. Lett. **B118** 124 (1981); M.Mangano, S. Parke, Fermilab-PUB-90/113-T (1990)

[17] G. Arnison et al., Phys. Lett. **B158** (1985) 494.

[18] R. Harris, (The CDF Collaboration), Proceed. of the Workshop on Hadron Structure Functions and Parton Distributions, Fermilab (1190), 278; Fermilab-CONF-90/118-E

[19] P. Aurenche et al., Fermilab-PUB-89/226-T (1989)